RSC Advances

ROYAL SOCIETY OF CHEMISTRY

www.rsc.org/advances

Journal Name

ARTICLE

Formation of PCDTBT:$PC_{71}BM$ p-n junction composite nanotubes via templating method

Received 00th January 20xx,
Accepted 00th January 20xx

DOI: 10.1039/x0xx00000x

www.rsc.org/

N. A. Bakar,[a] A. Supangat*[b] and K. Sulaiman[b]

The use of templating method to synthesize the p-n junction composite of poly [N-90-hepta-decanyl-2,7-carbazole-alt-5,5-(40, 70-di-2-thie-nyl 20, 10,30benzothiadiazole)] (PCDTBT): [6,6]-phenyl C_{71}-butyric acid methyl ester ($PC_{71}BM$) is reported in this study. These materials have been studied due to their potential applications in organic electronic based devices. Intimate contact between these materials can be realised via the facile fabrication of template-assisted method. Formation of p-n junction composite was elaborated in which its properties were compared over its bulk heterojunction counterparts. PCDTBT nanorods, nanotubes and nanoflowers were first produced followed by the infiltration of $PC_{71}BM$. Remarkable pattern at the first peak (carbazole) could be seen from the UV-vis spectra of PCDTBT:$PC_{71}BM$ p-n junction composite nanotubes at higher concentration of 15mg/ml. However, a reverse condition was occurred for its lower concentration of 5 mg/ml, which shown improvement at the second peak (DTBT) of UV-vis spectra. The first peak of 10 mg/ml solution concentration shows a wider peak compared to the 5 and 15 mg/ml concentrations with its second peak fallen between these two concentrations. Unlike the PCDTBT: $PC_{71}BM$ bulk-heterojunction whose shown a better quenching, PCDTBT: $PC_{71}BM$ composite nanotubes have shown a significant red-shifted in their photoluminescence (PL) spectra. Despite having a significant red-shifted, PCDTBT: $PC_{71}BM$ junction composites have shown poor quenching properties.

Introduction

Conjugated polymers have been broadly used in various technologies such as organic photovoltaic (OPV), organic light emitting diodes (OLED) and sensors due to their favourable properties.[1-4] These favourable properties are highly reliant on the preparation methods and the resultant nanostructures.[5, 6] Nanostructures of conjugated polymers such as nanorods, nanowires, nanoflowers and nanotubes[7-9] are some of the outstanding approaches in the development of versatile fabrications. The physical and chemical properties of polymers such as degree of polymerization, molar mass distribution, crystallinity and intermolecular properties can be altered by varying the fabrication techniques.

Poly [N-90-hepta-decanyl-2,7-carbazole-alt-5,5-(40,70-di-2-thie-nyl 20, 10,30benzothiadiazole)] (PCDTBT) is the most promising p-type conjugated polymer that possesses outstanding structural, optical and electronic properties.[1, 4, 6, 9, 10] Recently, PCDTBT has been extensively used as an active layer whether by incorporating it with n-type materials in bulk heterojunction system or as a single nanostructures material.[6, 9, 11] The synthesis of polymer composite at the nanoscale has received numerous attentions. Polymer composites that composed of both p- and n-type materials have a potential to enhance the charge carrier separation, charge carrier transfer and light absorption due to the formation of p-n junction[3, 4, 7, 11]

Template-assisted method is one of the considerable methods in fabricating the innumerable polymer composite architectures due to its mass production capabilities with minimal investment in cost and time.[6, 12-14] The most common techniques used in templating method are immersion (template wetting) and spin coating.[6, 7, 15, 16] A spin coating technique has been widely used in fabricating the bulk heterojunction based devices such as OPV, OLED and sensors by blending the p- and n-type materials.[4, 11, 17-19] By blending these materials, the interpenetrating structures are later produced, thus creating the bulk heterojunction system. Researchers have alternatively incorporated the conjugated polymer (p-type) and fullerenes (n-type), in order to provide charge transfer within the blends.[4, 20, 21] Practically, fullerenes such as [6,6]-phenyl C_{71}-butyric acid methyl ester ($PC_{71}BM$) and [6,6]-phenyl C_{61}-butyric acid methyl ester ($PC_{61}BM$) have an energetic deep lying LUMO which bestows the molecule with a high electron affinity relative to the various potential organic donors thus making it as an ideal n-type materials.[22, 23]

To the author best knowledge, studies involving one dimensional nanostructures of PCDTBT:fullerene junction composite have not been reported. Template-assisted method is useful in producing heterostructured composite via a simple layer by layer approach (two different materials incorporated together at a different time) such as composite nanotubes and nanorods.[3, 5, 7, 15] Since the charge separation of excitons is taking place at the interface between the p- and n- type, an intimate contact of both materials is required for the efficient splitting of the photogenerated excitons. To fulfil the vigorous charge carrier splitting, the large interfacial areas are highly needed, which in

[a] Department of Physics, Faculty of Science, University of Malaya, 50603 Kuala Lumpur, Malaysia
[b] Low Dimensional Materials Research Centre, Faculty of Science, University of Malaya, 50603 Kuala Lumpur, Malaysia. Email: azzuliani@um.edu.my; Fax: +60379674146; Tel: +60192682768

turns yielding the higher charge generation rates. Intimate contact at the nanoscale could be realized from the formation of p-n junction composite nanostructure. On the other hand, bulk heterojunction has been limited by its charge percolation within the intermixed phases. In this study, PCDTBT:$PC_{71}BM$ junction composite nanostructures and bulk heterojunction are compared in terms of their morphological, structural and optical properties by varying the spin coating rate and solution concentration. Formation of PCDTBT:$PC_{71}BM$ junction composite nanostructures via templating method is elaborated.

Experimental

PCDTBT and $PC_{71}BM$ were purchased from Luminescence Technology Corp (Taiwan, ROC) and Sigma Aldrich (St. Louis, USA), respectively, and used without further purification. PCDTBT and $PC_{71}BM$ were separately dissolved in chloroform for the solution concentration of 5 mg/ml (sample A), 10 mg/ml (sample B) and 15 mg/ml (sample C). For the bulk heterojunction samples, a blend mixture of PCDTBT:$PC_{71}BM$ with a ratio of 1:1 was also prepared for 5, 10 and 15 mg/ml. Porous alumina templates (Whatman Anodisc, Sigma-Aldrich,St. Louis, USA) and a glass substrates were used in synthesizing the p-n junction composite nanostructures and bulk heterojunction, respectively. The glass substrate (sail Brand, China) and porous alumina template were both cleaned by sonicating in acetone, ethanol and deionized water for 15 min prior to oven drying and nitrogen blowing.

PCDTBT:$PC_{71}BM$ junction composite nanotubes were prepared using the spin coating technique. 5, 10 and 15 mg/ml of PCDTBT solution was first spin coated onto the alumina template followed by the spin coated of 5, 10 and 15 mg/ml of $PC_{71}BM$ solution. Three different spinning rate of 1000 (sample 1), 2000 (sample 2) and 3000 rpm (sample 3) were applied throughout the coating. Afterwards, these samples were dried at room temperature prior to the dissolution process. Template dissolution was conducted for 12h by immersing the template in 4 M sodium hydroxide (NaOH). Meanwhile, the bulk heterojunction samples were prepared by blending the PCDTBT and $PC_{71}BM$ before the spin coating is taken place. Characterisations of their morphological, structural and optical properties were carried out by field emission scanning electron microscope (FESEM) (JSM 7600-F, JEOL Ltd., Tokyo, Japan), high resolution transmission electron microscope (HRTEM) (Hitachi HT7700, Japan), UV-vis spectroscope (Lambda 750, Perkin Elmer, Waltham, USA), photoluminescence spectroscope (Renishaw, Gloucestershire, UK) and Raman spectroscope.

Results and discussion

Fig. 1a, 1b, and 1c show the FESEM images of PCDTBT nanorods, nanotubes and nanoflowers that are produced from 5, 10 and 15 mg/ml solution concentration, respectively. These nanostructures are obtained after the dissolution of template prior to the infiltration of $PC_{71}BM$ solution. Fig. 2 shows the FESEM images of PCDTBT: $PC_{71}BM$ composites synthesized from 5 mg/ml solution concentration. Obviously, with the lower spin coating rate of 1000 rpm, most of the PCDTBT nanorods are intact, however, with less formation of p-n junction composite (Fig. 2a,b). Some of the nanorods are broken at the tips and collapsed to the non-aligned structures. The base is seen to be branched due to the existing branched structures of commercial porous alumina template. Both nanorods and nanotubes are visible, however, at spin coating rate of 1000 rpm the structures are dominated by nanotubes. Formation of nanorods is assumed to be originated from the PCDTBT itself. This assumption is due to the observation of PCDTBT nanorods that are confined inside the template before the dissolution process. Since, the low spin coating rate of $PC_{71}BM$ solution is applied, one could expect that high dissolution of $PC_{71}BM$ on the PCDTBT nanorods may have been occurred due to the usage of similar solvent (chloroform). Consistency of dissolution can be observed from the existence of composite nanorods at the branched bases. The spin coating rate could lead to the fast or slow solvent evaporation rate. At spin coating rate of 1000 and 2000 rpm, solvent has experienced a slow evaporation rate which could assist to the better ordered of polymer chain hence provide a morphology[24] improvement of PCDTBT:$PC_{71}BM$ p-n junction composite nanotubes. However, spin coating rate of 3000 rpm has fast solvent evaporation rate which could cause to the low degree of morphology. These explanations are supported by the FESEM images shown in Fig. 2c-f. At the spin coating rate of 2000 rpm (Fig. 2c,d), uneven penetration of $PC_{71}BM$ solution has occurred and the formation of p-n junction composite is observed. There are two different regions of bright and dark that corresponds to PCDTBT and $PC_{71}BM$, respectively. Higher spin coating rate of 3000 rpm has led to the formation of thin wall nanotubes that easily split and collapse during the dissolution process (shown by the red arrows in Fig. 2e). This phenomenon could be due to the low availability of PCDTBT solution at the beginning of the flow. It is believe that some of the solution has been splashed away during the infiltration process due to the high spin coating rate. Furthermore, low viscosity of 5 mg/ml solution also increases the possibility of splashing in a large amount. As shown in Fig. 2f, the flat tip of the remaining PCDTBT nanorods are observed although after the incorporation of $PC_{71}BM$ which further confirm the less availability of $PC_{71}BM$ solution during the higher spin coating rate of 3000 rpm.

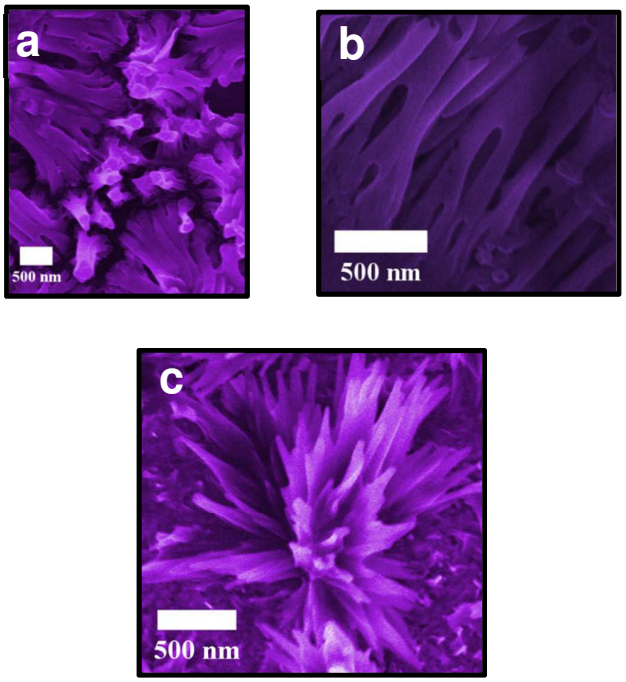

Fig. 1 FESEM images of PCDTBT nanorods (a), nanotubes (b) and nanoflowers (c).

Fig. 2 FESEM images of PCDTBT:$PC_{71}BM$ p-n junction composite of 5 mg/ml solution concentration at spin coating rate of 1000 rpm (a,b), 2000 rpm (c,d) and 3000 rpm (e-f).

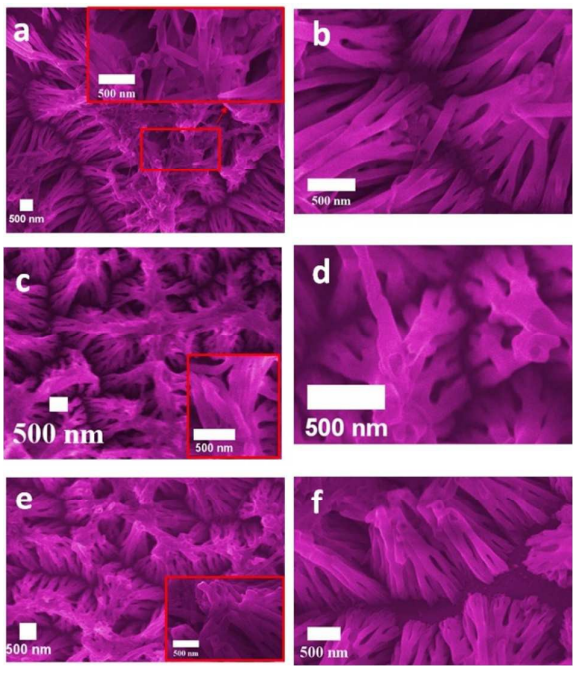

Fig. 3 FESEM images of PCDTBT: PC_{71} BM p-n junction composite of 10 mg/ml solution concentration at spin coating rate of 1000 rpm (a,b), 2000 rpm (c,d) and 3000 rpm (e,f).

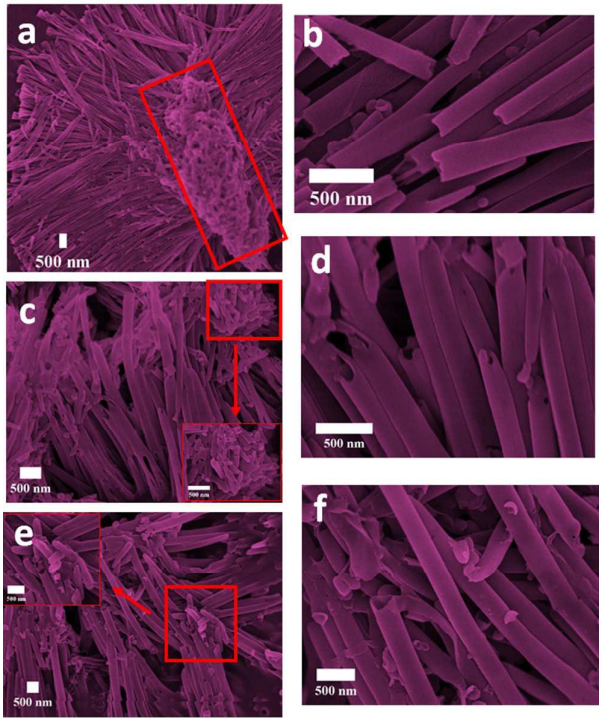

Fig. 4 FESEM images of PCDTBT:PC_{71} BM p-n junction composite of 15 mg/ml solution concentration at spin coating rate of 1000 rpm (a,b), 2000 rpm (c,d) and 3000 rpm (e,f).

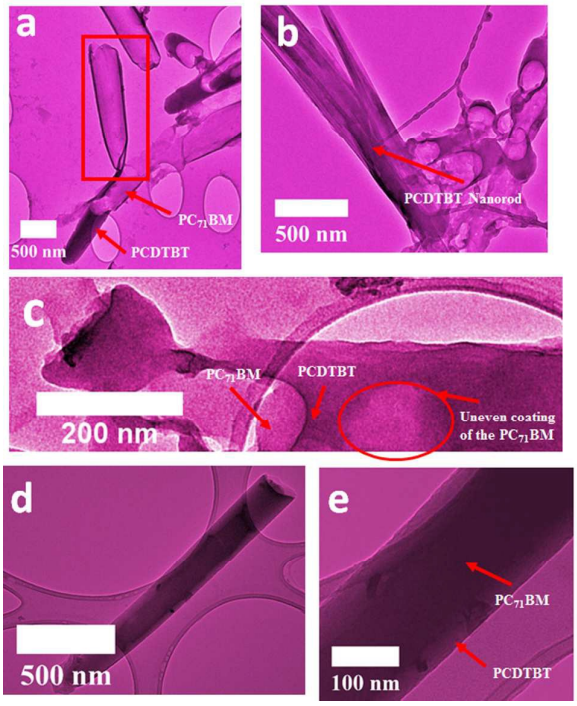

Fig. 5 HRTEM images of PCDTBT:PC_{71}BM p-n junction composite of 5mg/ml (a,b), 10mg/ml (c) and 15 mg/ml (d,e).

Fig. 3a,b, 3c,d and 3e,f show the FESEM images of PCDTBT:$PC_{71}BM$ p-n junction composite of 10 mg/ml solution concentration that fabricated at three different spin coating rate of 1000, 2000 and 3000 rpm, respectively. As can be seen from the images, higher spinning rate of 3000 rpm produced a shorter nanotubes compared to slower spinning rate of 1000 and 2000 rpm. The distance from the top to the Y-branched structure indicate the better infiltration portrayed by the lower spinning rate. Infiltration has happened throughout the channel which led to the longer nanotubes. As mentioned earlier, sufficient polymer supply that do not splash away at the beginning of spinning could contribute to the longer (higher aspect ratio) composite nanotubes which usually occur at a lower spinning rate. This reason could also contribute to the production of denser nanotubes (1000 rpm) which can be seen from the bigger island cause by a less collapsing nanotubes (due to the little space created between the nanotubes). Fig. 3a, c and e (inset) show the collapsed and agglomerated nanotubes at the tips due to the thin wall at the top (end of flowing).

Fig. 4a,b, 4c,d and 4e,f show the FESEM images of PCDTBT:$PC_{71}BM$ p-n junction composite of 15 mg/ml solution concentration that fabricated at three different spin coating rate of 1000, 2000 and 3000 rpm, respectively. The p-n junction composite nanotubes that have been synthesized at higher solution concentration exhibit the longer and less broken (stable) structures if compared to the structures that synthesized at lower solution concentration. As reported elsewhere[25] higher solution concentration of higher viscosity would give a better infiltration and aspect ratio. Viscous solution could prevent the polymer from splashing in a large amount during the spinning unlike the less viscous solution which tends to easily splash away. Therefore, more viscous solution will provide a huge availability of polymer solution to undergo infiltration process. In addition, a viscous polymer solution will give a thicker PCDTBT:$PC_{71}BM$ composite nanotubes' wall which could direct to the stable and less broken nanotubes. Distance of travelling solution throughout the porous nanochannel (template) will indicate the thickness of nanotubes' walls. As the solution travelling deeper into the nanochannel, the nanotubes' walls will tend to get thinner. Fig. 4a shows the agglomeration and joining tips of composites due to the extreme thinner walls which do not break but tend to collapse with each other during dissolution process. On the other hand, Fig. 4c and 4e show the formation of meniscus tips with less visible agglomeration, which may be due to the high spin coating rate. Theoretically, solution has a tendency to splash away in a large amount of solution and allow only small presence of polymer solution for the infiltration. This phenomenon is supported by Fig. 4b, 4d and 4f in which broken nanotubes are likely to form with the spin coating rate of 1000 rpm. The higher spin coating rate produced slightly thicker walls than the former and has contributed to a more stable structures with prevention of agglomerated tips (despite of being broken at the meniscus). Most of the nanotubes are broken at the tips meniscus due to the formation of thinner wall at the end of the flowing (tip) compared to the thicker at the base which acts as the starting point of flown fluid. Fast evaporation rate and decreased amount of polymer solutions[26] at the tips during the nanotubes growth could also cause to the thinning of walls.

HRTEM images of individual PCDTBT:$PC_{71}BM$ p-n junction composite nanotubes of 5, 10 and 15 mg/ml solution concentration are shown in Fig. 5a,b, 5c and Fig. 5d,e, respectively. HRTEM image of 5 mg/ml PCDTBT:$PC_{71}BM$ composite nanotubes (Fig. 5a) is well correlated with their FESEM images shown in Fig. 2d with the appearance of dissolution by $PC_{71}BM$ solution. HRTEM image in Fig. 5b confirms the presence of PCDTBT nanorods which originated from the confined PCDTBT that exempted from the dissolution by $PC_{71}BM$. The HRTEM image of 10mg/ml based p-n junction composite nanotubes shows some uneven coating of $PC_{71}BM$ on the surface of PCDTBT layer. 15 mg/ml based p-n junction composite nanotubes garnered a better stability of definite nanotubes (Fig. 5c,d). The outer (PCDTBT) and inner layer ($PC_{71}BM$) of composite nanotubes show the consecutive formation of p-n junction due to the incorporation of spin-coated $PC_{71}BM$. Two different regions of brighter and darker can be seen in the PCDTBT:$PC_{71}BM$ composite nanotubes of all solution concentrations which represents PCDTBT and $PC_{71}BM$, respectively.

Fig. 6a, 6b and 6c illustrate the formation of 5, 10 and 15 mg/ml of PCDTBT:$PC_{71}BM$ p-n junction composite and the structures' transition due to the spin-coated of $PC_{71}BM$ onto the confined PCDTBT nanorods, respectively, based on the general observations made from FESEM and HRTEM images. Due to the usage of similar solvent (chloroform) for both PCDTBT and $PC_{71}BM$, the existing formation of confined p-type has been distorted by the n-type solution. Although, the different spin coating rates of 1000, 2000 and 3000 rpm are applied for only 30s during the deposition of n-type, it is enough to just dissolve a middle part of the confined PCDTBT to become a porous structure. Consequently, $PC_{71}BM$ will be able to infiltrate into the p-type and forms PCDTBT:$PC_{71}BM$ junction composite nanotubes. The faster evaporation rate and stronger adhesive forces have also promote the formation of PCDTBT:$PC_{71}BM$ junction composite nanotubes and inhibit the complete infiltration of the polymer solution. Fig. 6a (i-vi) shows the illustration of uneven distribution of $PC_{71}BM$ after the dissolution of template which likely to occur with the lower solution concentration of 5 mg/ml. The spin coating techniques used to deposit both p- and n-type and less viscous solution (5mg/ml) could be the ultimate reasons for the formation of thinner wall. Immersion technique followed by spin coating technique of the same concentration of 5 mg/ml has been reported to exhibit more stable nanotubes[7]. The sufficient time provided by the immersion technique has enhanced the wetting and coating thickness of polymer solution on the template's wall. Some of the PCDTBT nanorods remain as they were although the incorporation of $PC_{71}BM$ has occurred. Fig 6b (i-v) elucidates the formation of 10 mg/ml of PCDTBT:$PC_{71}BM$ p-n junction composite and the coating mechanism of $PC_{71}BM$ on the inner surface of PCDTBT nanotube. Instead of solid nanostructure (nanorods and nanoflowers), 10 mg/ml has produced a hollow PCDTBT nanostructure (nanotubes). The different spinning rate of 1000, 2000 and 3000 rpm of $PC_{71}BM$ solution will help to coat the PCDTBT nanotubes' inner layer in spiral motion and led to the uneven coating as shown in the HRTEM image of Fig. 5c. 15 mg/ml of solution concentration has improved the morphology of PCDTBT:$PC_{71}BM$ composite nanotubes (Fig. 6c(i-vi)). Incorporation of $PC_{71}BM$ into the PCDTBT nanorods that confined inside the template's channel has caused some changes on the physical properties of the final formation of PCDTBT: $PC_{71}BM$.The thinning of the nanotube's wall as the solution flows through the channel occurred for all concentrations of 5, 10 and 15 mg/ml.

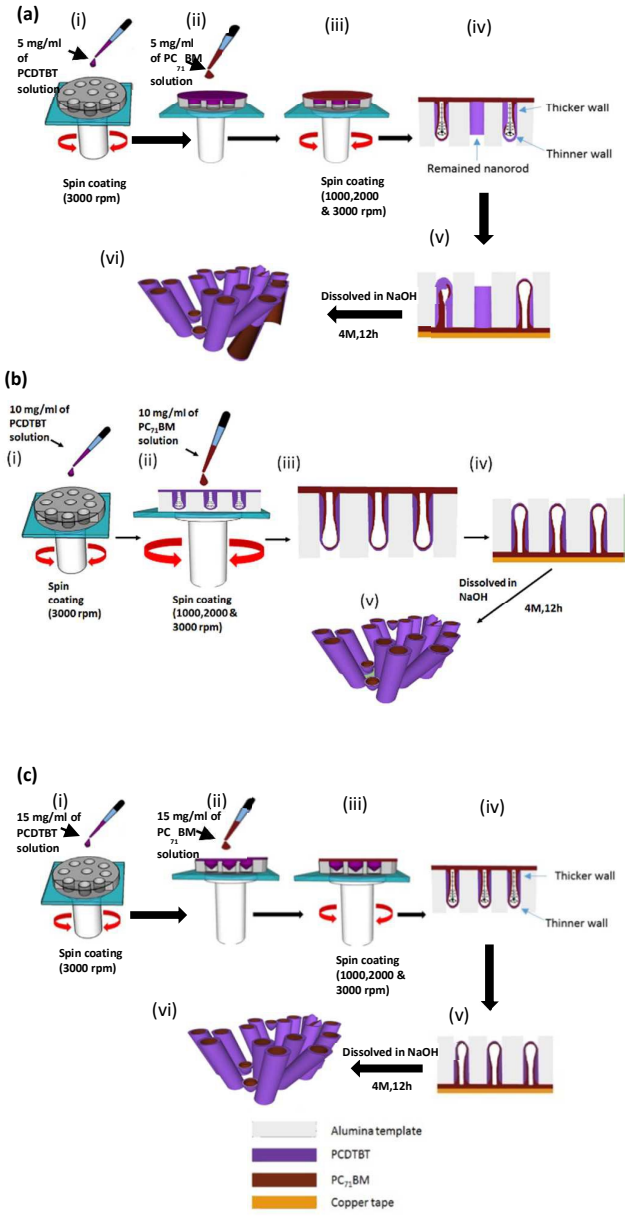

Fig. 6 Schematic illustration of the formation of PCDTBT:$PC_{71}BM$ composite nanotubes of 5 mg/ml (a), PCDTBT:$PC_{71}BM$ composite nanotubes of 10 mg/ml (b), PCDTBT:$PC_{71}BM$ composite nanotubes of 15 mg/ml (c).

Fig. 7 shows the UV-vis spectra of $PC_{71}BM$ thin film, PCDTBT thin film and PCDTBT:$PC_{71}BM$ bulk heterojunction of different solution concentrations and spin coating rate. PCDTBT thin film has portrayed the significant peaks absorption between 350-650 nm at UV and visible region which represent the carbazole (Cz) donor and dithienylbenzothiadiazole (DTBT) acceptor, respectively. UV-vis spectrum of PCDTBT thin film portrayed a broad valley between 400-500 nm while the UV-vis spectrum of $PC_{71}BM$ thin film shows its main peak absorption between 450-500 nm. It can be observed that, the main peak of DTBT located at 580 nm decrease its intensity, while the middle valley (500 nm) showed an increased intensity after the incorporation of PCDTBT and $PC_{71}BM$ for both concentrations (5 and 15 mg/ml) which represent the mixed state of the two parent materials. By incorporating these two materials, a broader absorption peak at a visible region can be recognized. Solution concentration has played a vital role in giving the significant difference in term of optical properties (wider absorption band at a longer wavelength), in which 5 mg/ml of bulk heterojunction film shows a red-shifted and wider absorption if compared to its 15 mg/ml. The solution concentration and polymer-fullerene ratio have enforced a strong influence on the aggregation behaviour of the blends which are related to the red-shift (absorption edge transition) of the optical absorption spectra.

Fig. 8a shows the absorption spectra of PCDTBT nanoflowers and PCDTBT nanorods which is well correlated with the previous report.[6] UV-vis absorption spectrum of PCDTBT nanoflowers shows a red-shifted and wider absorption at its second peak whereas UV-vis absorption spectrum of PCDTBT nanorods shows a red-shifted at its first peak. Absorption edge of PCDTBT nanotubes (10 mg/ml) is consistent with PCDTBT nanorods (5 mg/ml) and nanoflowers (15 mg/ml) which fall between these two concentrations. Optical properties between 5 mg/ml of PCDTBT:$PC_{71}BM$ composite nanotubes and its bulk heterojunction films are compared (Fig. 8b). PCDTBT:$PC_{71}BM$ bulk heterojunction films exhibited a prominent intensity and red-shift at its second peak. However, a wider peak absorption is dominated by PCDTBT:$PC_{71}BM$ composite nanotubes of all spin coating rates. Wider peak absorption also can be seen for 10 mg/ml composite nanotubes as compared to its bulk heterojunction (Fig. 8c). As an overall, the higher solution concentration of PCDTBT:$PC_{71}BM$ composite nanotubes has shown a better optical absorption across of all spectra than its bulk heterojunction films counterpart (Fig. 8d). Remarkable pattern of peak absorption of bulk heterojunction for all three concentrations (5, 10 and 15 mg/ml) can be clearly seen from the UV-vis spectra which show a prominent peak intensity and peak narrowing beyond its composite nanotubes. However, the widening of peak absorption is dominated by the composite nanotubes of all solution concentrations. The PCDTBT:$PC_{71}BM$ composite nanotubes of 15 mg/ml has a dominant red-shifted at its first peak which corresponds to the Cz donor (Fig. 8e). Although, a red-shifted at its second peak has not occurred, a wider absorption of second peak is clearly seen. PCDTBT:$PC_{71}BM$ composite nanotubes of 5 mg/ml shows a significant absorption edge transition to a longer wavelength (red shift) at its second peak which corresponds to the DTBT acceptor. If comparison to be made in terms of the red-shifted at the second peak between the composite nanotubes and bulk heterojunction films, the latter seems to exhibit a promising shifted.

$PC_{71}BM$ has acted as a defect site[24] which disrupt the ordering packing of the PCDTBT chain during the solvent removal process. Disruption is increased with the increasing of $PC_{71}BM$ amount which then decrease the conjugation length or blue-shifted. Changes of dominancy of peak absorption is realised by changing the solution concentration of composite nanotubes. A low concentration of polymer-fullerene system has a wider absorption range at the longer wavelength[27] due to the suppress of $PC_{71}BM$ aggregates growth in low concentration which caused the optimise and stable phase separation between interfaces.[24] Solution concentration of polymer imposed a strong influence on the aggregation behaviour and significantly related to the red-shifted of UV-vis absorption peak. Within polymer-fullerene system, the probability for the polymer solution to entangle is reduced in diluted solution and promotes the formation of aggregates. Diluted solution has a higher degree of freedom (to flow) which enables aggregation, while the probability for the polymer solution to entangle increase in higher concentration solution which precludes the formation of aggregates.[27]

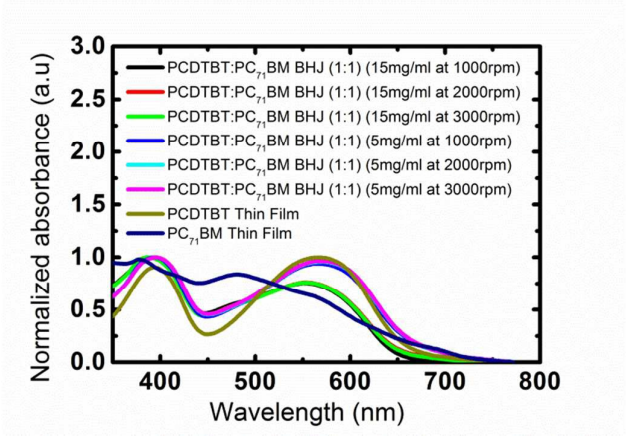

Fig. 7 UV-vis absorption spectra of PCDTBT thin film, $PC_{71}BM$ thin film and PCDTBT:$PC_{71}BM$ bulk heterojunction of 5 and 15 mg/ml of 1000, 2000 and 3000 rpm.

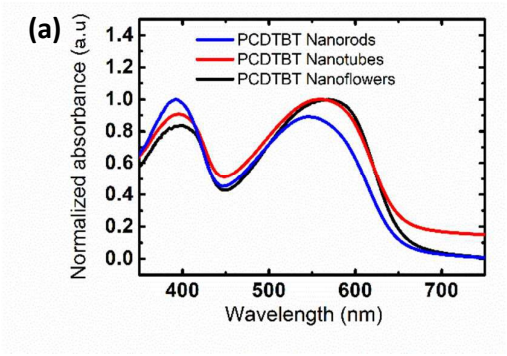

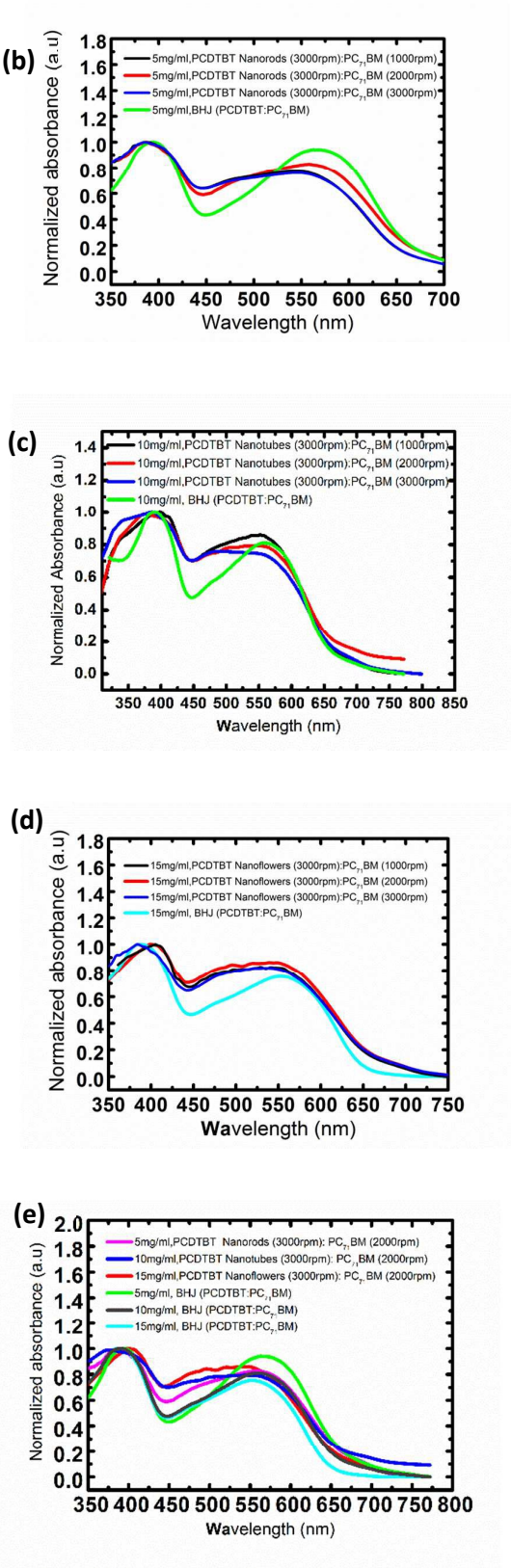

Fig. 8 UV-vis absorption spectra of PCDTBT nanorods, nanotubes and nanoflowers (a), PCDTBT:$PC_{71}BM$ composite nanotubes and

bulk heterojunction of 5 mg/ml (b), PCDTBT:$PC_{71}BM$ composite nanotubes and bulk heterojunction of 10 mg/ml (c), PCDTBT:$PC_{71}BM$ composite nanotubes and bulk heterojunction of 15 mg/ml (d) and PCDTBT:$PC_{71}BM$ composite nanotubes of 5, 10 and 15 mg/ml (e).

Fig. 9a shows the PL spectra of PCDTBT nanorods, PCDTBT nanotubes and PCDTBT nanoflowers. Not much quenching is seen apart of the shifting in peak for PCDTBT nanotubes and PCDTBT nanoflowers. Significant quenching can be seen for PCDTBT nanotubes compared to PCDTBT nanorods and nanoflowers. PCDTBT nanoflowers (peak at 701 nm) has slightly undergone a red-shifted whereas PCDTBT nanorods (peak at 692 nm) has a slight quenched.[6] Between these three PCDTBT nanostructures, PCDTBT nanoflowers show the most significant shifting to the lower energy. As shown in Fig. 9b, 9c and 9d, PL spectra of composites exhibited a prominent difference compared to the single material. PCDTBT:$PC_{71}BM$ composite nanotubes shown a favourable luminescence properties of quenching and shifting compared to the single material of PCDTBT nanorods, PCDTBT nanotubes and PCDTBT nanoflowers. PCDTBT:$PC_{71}BM$ composite nanotubes of 5 mg/ml that spin coated at 1000, 2000 and 3000 rpm exhibited the maximum PL peak at 714, 715 and 712 nm, respectively. Meanwhile, PCDTBT:$PC_{71}BM$ composite nanotubes of 10 mg/ml that spin coated at 1000, 2000 and 3000 rpm exhibited the maximum PL peak at 720, 721 and 719 nm, respectively. PL peak at 722, 718 and 721 nm displayed by PCDTBT:$PC_{71}BM$ composite nanotubes of 15 mg/ml that spin coated at 1000, 2000 and 3000 rpm, respectively. Quenching of PL spectra of PCDTBT:$PC_{71}BM$ composite nanotubes is related to the photo-induced charge separation between electron donor (PCDTBT) and electron acceptor ($PC_{71}BM$) molecules. The presence of $PC_{71}BM$ (guest) will facilitates the energy flow and sanctions the role of inter and intrachain energy transfer to be efficiently separated.[28] Additionally, the thin wall of nanotubes offers a short distance to facilitate ion transport while hollow nanotubes permit counter ions to readily penetrate into the composite material.[26] However, bulk heterojunction films of all concentrations (5, 10 and 15mg/ml) having a more significant quenching if compared with the composite nanotubes (Fig. 9e). Higher emission peaks would suggest to the radiative recombination and sub-optimal nanostructures within the composite nanotubes system. Strong surface tension generated at the interface between the nanotubes and solvent during solvent evaporation and dissolution processes could be one of the greatest contributors to the sub-optimal nanostructures. On the other hand, the red-shifted of PL spectra at 714, 720 and 722 nm in composite nanotubes system is due to the increased in the Stokes shift which also implies that the polymer chain become more rigid. The increase in rigidity is well associated with the better alignment state of polymer chains in the porous alumina template.[29, 30] The extra longer chains allowed the higher diffusion rate of $PC_{71}BM$ into the PCDTBT due to the increase of interspacing between backbones, which resulted in larger scale phase separation between compounds.[31] This could be the main reason to the red-shifted of composite nanotubes but less quenched if compared to its bulk heterojunction films.

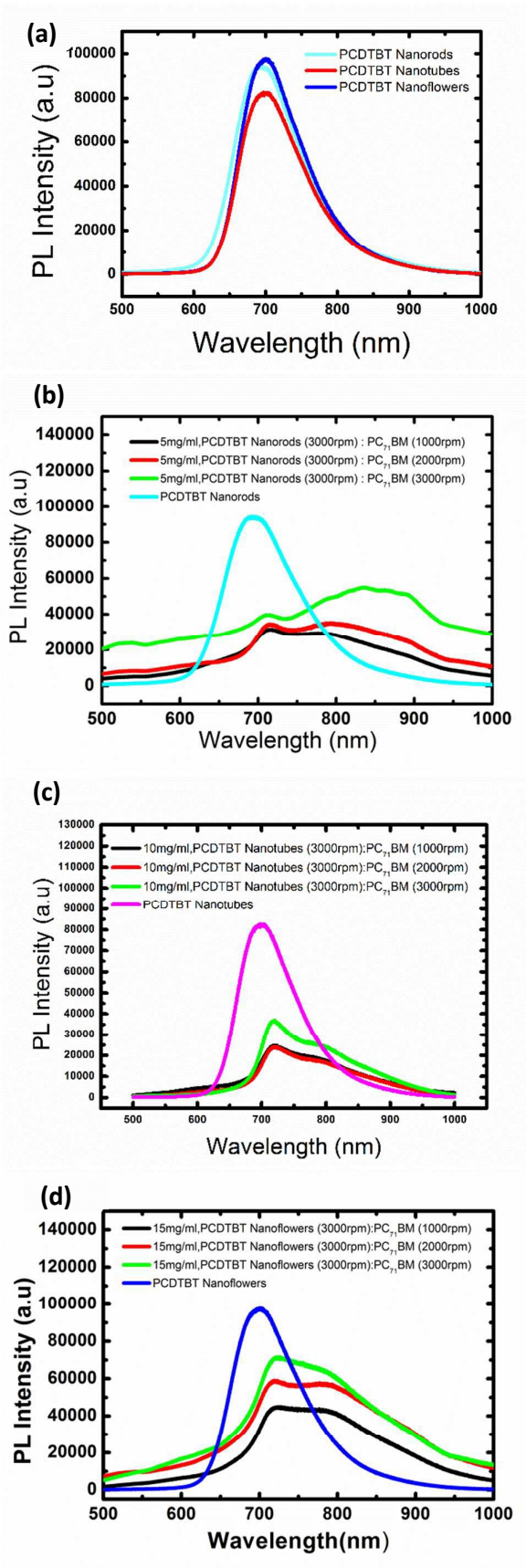

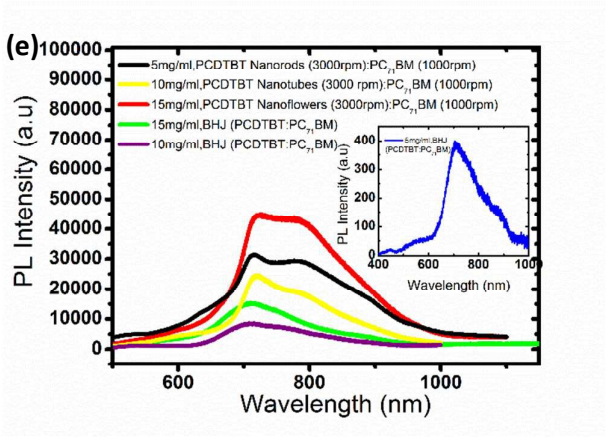

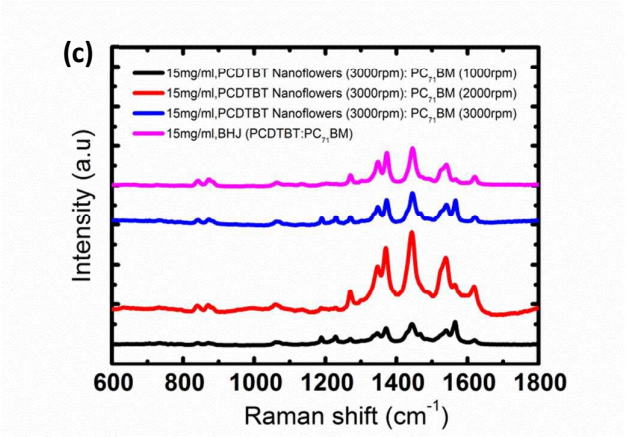

Fig. 9 PL spectra of PCDTBT nanorods, nanotubes and nanoflowers (a), PCDTBT:$PC_{71}BM$ composite nanotubes of 5 mg/ml and PCDTBT nanorods (b), PCDTBT:$PC_{71}BM$ composite nanotubes of 10 mg/ml and PCDTBT nanotubes (c), PCDTBT:$PC_{71}BM$ composite nanotubes of 15 mg/ml and PCDTBT nanoflowers (d) and PCDTBT:$PC_{71}BM$ composite nanotubes and bulk heterojunction films (e).

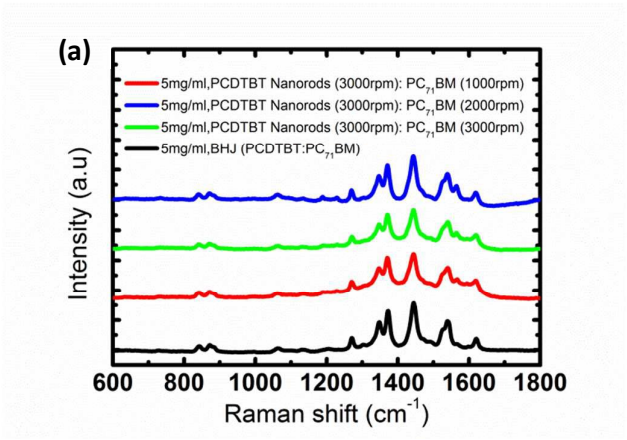

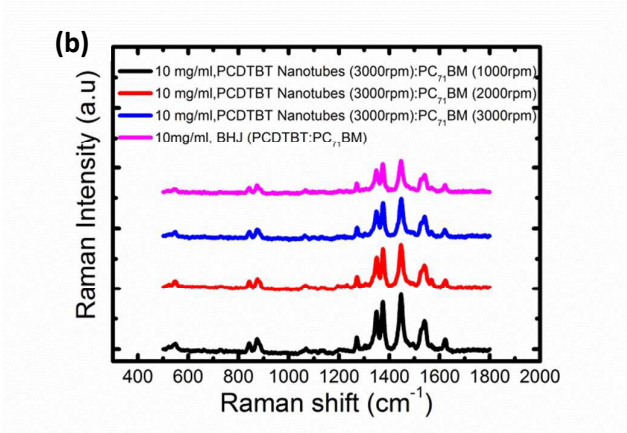

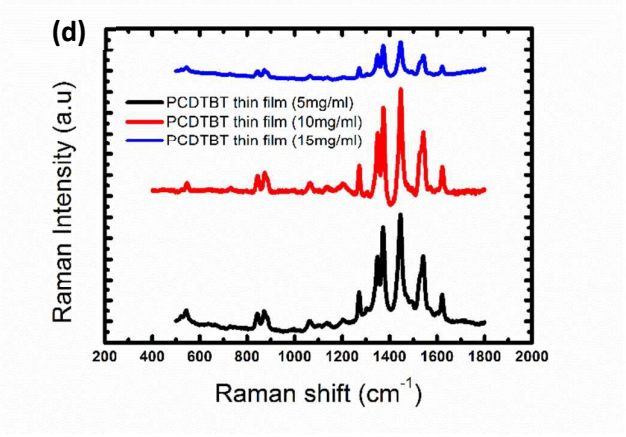

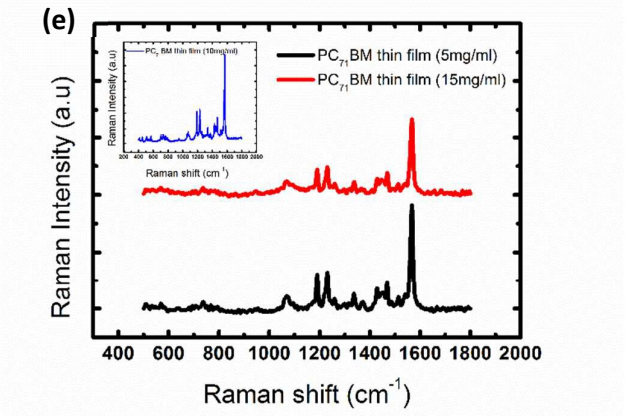

Fig. 10 Raman spectra of PCDTBT:$PC_{71}BM$ composite nanotubes and bulk heterojunction films of 5 mg/ml (a), PCDTBT:$PC_{71}BM$ composite nanotubes and bulk heterojunction films of 10 mg/ml (b), PCDTBT:$PC_{71}BM$ composite nanotubes and bulk heterojunction films of 15 mg/ml (c), PCDTBT thin films of 5, 10 & 15 mg/ml (c) and $PC_{71}BM$ thin films of 5,10 & 15 mg/ml (d).

Fig. 10 a,b,c,d show the Raman spectra of 5 mg/ml PCDTBT:$PC_{71}BM$ composites nanotubes & its bulk heterojunction films, 10 mg/ml PCDTBT:$PC_{71}BM$ composites nanotubes & its bulk heterojunction films, 15 mg/ml PCDTBT:$PC_{71}BM$ composites nanotubes & its bulk heterojunction films and PCDTBT & PCBM thin films, respectively. Comparison of Raman spectra between PCDTBT thin films and $PC_{71}BM$ thin films have shown that there are peaks exist for $PC_{71}BM$ but not in PCDTBT which assigned for C-H bending at 1191 and 1231cm^{-1}, pentagonal pinch modes of the fullerenes at 1569 cm^{-1} and Raman actives modes of the fullerenes at 1568 cm^{-1}. There are some peaks arise for PCDTBT molecule motion that located at 843, 871, 1065, 1271, 1349, 1373, 1445, 1541, and 1622 cm^{-1} which are well correlated with the previous reports[6, 9, 32]. These peaks are assigned for symmetric C-S stretch, asymmetric C-S stretch, localized mode characterized by C-H in-plane bending together with the C=C stretch at the thiophene ring, C-H in plane bending and C=C stretch bending of the benzothiadiazole delocalized mode as well as C-H in plane bending with the C=C stretch for both carbazole and thiophene unit, delocalized motion involving benzothiadiazole, thiophene, and carbazole unit for 1349 and 1373 cm^{-1}, localized motion involving carbazole, thiophene and benzothiadiazole, localized motion involving carbazole unit only, localized motion involving benzothiadiazole unit only and localized motion involving carbazole unit which is related to the C-H in plane bending together with C=C stretch.

Assignments and changes in the wavenumber band between PCDTBT:$PC_{71}BM$ composite nanotubes, bulk heterojunction thin films and PCDTBT & $PC_{71}BM$ thin film are tabulated in Table 1, 2 and 3, respectively. 15 mg/ml of PCDTBT thin film shown the slightly upward shift of several peaks that represent symmetric & asymmetric C-S stretch, localized motion involving carbazole unit (C-H bending, C=C stretch, C-N stretch and C-H in plane bending) & thiophene unit (C-H bending and C=C stretch) and symmetric C=C & C-H in plane bending of the carbazole part which can be related to the change in the bond order of PCDTBT chain backbone.[32] Other peaks at 1065, 1271, 1349 and 1373 cm^{-1} remain unchanged for both 5 and 15 mg/ml PCDTBT thin film that are assigned for C-H in plane bending + C=C stretch of localized thiophene unit, C-H bending + C=C stretch on benzothiadiazole, carbazole and thiophene unit, C-H bending of benzothiadiazole + thiophene or C=C stretch on carbazole + benzothiadiazole unit and benzothiadiazole, thiophene, carbazole C=C stretching + C-H in plane bending or C-N stretch of carbazole unit.

With the ratio of 1:1, the less viscous $PC_{71}BM$ solution has caused the peaks to diminish in its bulk heterojunction films. Upward shift of 15 mg/ml bulk heterojunction films for C-S stretch, C-H in plane bending as well as C=C stretch in thiophene unit, C-H bending of delocalized benzothiadiazole or thiophene segment and C=C stretch of benzothiadiazole including carbazole could be attributed to the better molecular arrangement exhibited by higher concentration and also shift of the electron density from the carbazole to the acceptor moiety thus lengthening the carbazole C-C bonds.[32] There are no changes in peaks position that assigned for asymmetric C-S stretch (873 cm^{-1}), carbazole C-N stretch (1373 cm^{-1}), C=C stretch and C-H in plane bending of delocalized benzothiadiazole, carbazole and thiophene unit (1261 and 1271 cm^{-1}).

Downward in Raman shift expresses that incorporation of $PC_{71}BM$ has an impact on the molecular structural reorganization of the PCDTBT. Raman peak at 1191 cm^{-1} which is assigned for C-H bending ($PC_{71}BM$ thin film) is only appeared in 15 mg/ml PCDTBT:$PC_{71}BM$ composite nanotubes which band is at 1189 and 1190 cm^{-1}. Raman shift at 1231 cm^{-1} which indicates the C-H bending in $PC_{71}BM$ molecular structures has only existed in 15 mg/ml PCDTBT:$PC_{71}BM$ composite nanotubes and diminished for 5mg/ml PCDTBT:$PC_{71}BM$ composite nanotubes. C-H bending has undergone a downward shift of ~ 3 cm^{-1} and 2 cm^{-1} to 1228 and 1229 cm^{-1} for 15 mg/ml PCDTBT:$PC_{71}BM$ composite nanotubes. Raman shift at 1470 cm^{-1} of higher concentration is seen for pentagonal pinch modes of the fullerenes which also occurred in 15 mg/ml PCDTBT:$PC_{71}BM$ composite nanotubes with a downward shift of 1467 and 1468 cm^{-1}. The Raman actives modes of fullerenes that occurred at 1568cm^{-1} [33] is similar for both concentrations. Downward shift in Raman peaks of almost all PCDTBT peaks after the incorporation of $PC_{71}BM$, indicate the strong influence of $PC_{71}BM$ on the molecular level of PCDTBT and vice versa. Significant downward shift of all $PC_{71}BM$ peaks after incorporated with PCDTBT, specify the impact of PCDTBT on the molecular level of $PC_{71}BM$. Peaks that represent the $PC_{71}BM$ have only existed at the higher concentration of 15 mg/ml PCDTBT:$PC_{71}BM$ composite nanotubes except for the Raman actives mode of fullerene which exist for all concentrations. Peaks that assigned for different molecular alterations have arisen due to the formation of PCDTBT:$PC_{71}BM$ composite nanotubes.

Delocalized benzothiadiazole + thiophene C-H bending and carbazole + benzothiadiazole C=C stretch offer significant downward shift of ~2 cm^{-1} for PCDTBT:$PC_{71}BM$ composite nanotubes and not for their bulk heterojunction films. The same goes for C=C stretch + C-H in plane bending of delocalized benzothiadiazole + thiophene + carbazole and carbazole C-N stretch which shift is only existed for composite nanotubes. 15 mg/ml of PCDTBT:$PC_{71}BM$ composite nanotubes has experienced a significant downward shift of ~3 cm^{-1} (1619 cm^{-1}) and 2 cm^{-1} (1621 cm^{-1}), ~2 cm^{-1} (1620 cm^{-1}) for 10 mg/ml, while 5 mg/ml of PCDTBT:$PC_{71}BM$ composite nanotubes shift to 1619 cm^{-1} and 1620 cm^{-1} from 1622 cm^{-1}.

Table 1 Raman peak position of PCDTBT:$PC_{71}BM$ composite nanotubes of 5 and 15 mg/ml. bulk heterojunction thin films of 5, 10 and 15 mg/ml.

Raman shift (cm^{-1})									
PCDTBT:$PC_{71}BM$ composite nanotubes									Assignments
5 mg/ml			10 mg/ml			15 mg/ml			
A1	A2	A3	B1	B2	B3	C1	C2	C3	
842	842	841	843	843	844	841	842	842	Sym C-S stretch
871	871	871	875	876	874	872	870	873	Asym C-S strecth
1062	1062	1065	1069	1067	1064	1062	1063	1066	L: Th CH ip δ+Vc=c
-	-	-	-	-	-	1189	-	1190	C-H δ
-	-	-	-	-	-	1228	-	1229	C-H δ
1271	1270	1271	1270	1271	1271	1270	1270	1271	D: BT δ +Vc=c+C-H ip δ, Cz+Th CH ip δ+ V c=c
1347	1347	1347	1350	1350	1349	1346	1347	1347	D: BT+Th CH δ, Cz+BT Vc=c
1371	1371	1372	1375	1375	1375	1371	1371	1373	BT+Th+Cz Vc=c+,C-H in plane δ,CZ V_{C-N}
1445	1444	1444	1447	1446	1448	1444	1444	1445	L:Cz Th Vc=c + CH ip δ, Cz V_{C-N}
-	-	-	-	-	-	1467	-	1468	Pentagonal pinch modes of the fullerenes
1540	1540	1540	1540	1540	1541	1540	1538	1541	L:BT+Th sym Vc=c, CH ip δ
1568	1566	1565	1567	1568	1567	1566	1564	1567	Antisymmetric stretch modes of the fullerene
1619	1619	1620	1624	1624	1620	1621	1619	1621	L:Cz Vc=c+CH ip δ
Sym, symmetric; asym, asymmetric; L, localized; Th, thiophene; ip,in plane; Va-b, stretch of a-b bond; δ, bend; D, delocalized; BT, benzothiadiazole; Cz, carbazole									

Table 2 Raman peak position of PCDTBT:$PC_{71}BM$ bulk heterojunction thin films of 5, 10 and 15 mg/ml.

Raman shift (cm^{-1})			
BHJ			
5 mg/ml	10 mg/ml	15 mg/ml	Assignments
841	842	842	Sym C-S stretch
873	874	873	Asym C-S strecth
1064	1065	1065	L: Th CH ip δ+Vc=c
1271	1270	1271	D: BT δ +Vc=c+C-H ip δ, Cz+Th CH ip δ+ V c=c
1348	1349	1349	D: BT+Th CH δ, Cz+BT Vc=c
1373	1374	1373	BT+Th+Cz Vc=c+,C-H in plane δ,CZ V_{C-N}
1445	1447	1446	L:Cz Th Vc=c + CH ip δ, Cz V_{C-N}
1539	1540	1541	L:BT+Th sym Vc=c, CH ip δ
-	-	-	Antisymmetric stretch modes of the fullerene
1621	1622	1621	L:Cz Vc=c+CH ip δ
Sym, symmetric; asym, asymmetric; L, localized; Th, thiophene; ip,in plane; Va-b, stretch of a-b bond; δ, bend; D, delocalized; BT, benzothiadiazole; Cz, carbazole			

Table 3 Raman peak position of PCDTBT and $PC_{71}BM$ thin films of 5, 10 and 15 mg/ml.

Raman shift (cm^{-1})						
$PC_{71}BM$ Thin film			PCDTBT Thin film			Assignments
5 mg/ml	10 mg/ml	15 mg/ml	5 mg/ml	10 mg/ml	15 mg/ml	
-	-	-	843	844	844	Sym C-S stretch
-	-	-	871	874	873	Asym C-S stretch
1070	1073	1071	1065	1065	1065	L: Th CH ip δ+Vc=c
1191	1190	1191	-		-	C-H δ
1231	1231	1231	-		-	C-H δ
-	-	-	1271	1272	1271	D: BT δ +Vc=c+C-H ip δ, Cz+Th CH ip δ+ V c=c
-	-	-	1349	1350	1349	D: BT+Th CH δ, Cz+BT Vc=c
-	-	-	1373	1374	1373	BT+Th+Cz Vc=c+,C-H in plane δ,CZ V_{C-N}
-	-	-	1445	1447	1446	L:Cz Th Vc=c + CH ip δ, Cz V_{C-N}
1469	1469	1470	-		-	Pentagonal pinch modes of the fullerenes
-	-	-	1541	1542	1542	L:BT+Th sym Vc=c, CH ip δ
1568	1568	1568	-		-	Antisymmetric stretch modes of the fullerene
-	-	-	1622		1623	L:Cz Vc=c+CH ip δ
Sym, symmetric; asym, asymmetric; L, localized; Th, thiophene; ip,in plane; Va-b, stretch of a-b bond; δ, bend; D, delocalized; BT, benzothiadiazole; Cz, carbazole						

Conclusions

In this work, PCDTBT:$PC_{71}BM$ p-n junction composite nanotubes have been synthesized via a templating method of spin coating technique by a simple layer by layer approach. Optimum concentration of single and composites materials has been revealed. With comparison to 3000 rpm, spin coating rate of 1000 and 2000 rpm produce a more stable composite nanotubes for all concentrations of 5, 10 and 15 mg/ml. The stability of the composite nanotubes increases as the concentrations increase. Higher concentration of 15 mg/ml produces more definite and less broken composite nanotubes. PCDTBT:$PC_{71}BM$ p-n junction composite nanotubes have a better light absorption properties in a wide spectral range and its bulk heterojunction films shows a better photo-induced charge transfer.

Acknowledgements

We would like to acknowledge the University of Malaya for the project funding under the University Malaya Postgraduate Research Grant (PG093-2014A), the University of Malaya High Impact Research Grant UM-MoE (UM.S/625/3/ HIR/MoE/SC/26), and the Ministry of Education Malaysia for the project funding under the Fundamental Research Grant Scheme (FP002-2013A).

Notes and references

1. P. Jha, S. P. Koiry, V. Saxena, P. Veerender, A. Gusain, A. K. Chauhan, A. K. Debnath, D. K. Aswal and S. K. Gupta, *Organic Electronics*, 2013, 14, 2635-2644.
2. J. Y. Lek, Y. M. Lam, J. Niziol and M. Marzec, *Nanotechnology*, 2012, 23, 315401.
3. J. Yan, Q. Ye, X. Han and F. Zhou, *RSC Advances*, 2013, 3, 166–171.
4. S. Kannappan, K. Palanisamy, J. Tatsugi, P.-K. Shin and S. Ochiai, *Journal of Materials Science*, 2012, 48, 2308-2317.
5. Z. Xiang, H. Sun, Z. Zhu, W. Liang, B. Yang and A. Li, *RSC Advances*, 2015, 5, 24893–24898.
6. N. A. Bakar, A. Supangat and K. Sulaiman, *Materials Letters*, 2014, 131, 27-30.
7. A. H. Ahmad Makinudin, M. S. Fakir and A. Supangat, *Nanoscale Research Letters*, 2015, 10.
8. M. S. Fakir, A. Supangat and K. Sulaiman, *Journal of Nanomaterials*, 2014, 2014, 1-7.
9. N. A. Bakar, A. Supangat and K. Sulaiman, *Nanoscale research letters*, 2014, 9, 600.
10. N. Banerji, E. Gagnon, P.-Y. Morgantini, S. Valouch, A. R. Mohebbi, J.-H. Seo, M. Leclerc and A. J. Heeger, *The Journal of Physical Chemistry C*, 2012, 116, 11456-11469.
11. T. M. Clarke, J. Peet, A. Nattestad, N. Drolet, G. Dennler, C. Lungenschmied, M. Leclerc and A. J. Mozer, *Organic Electronics*, 2012, 13, 2639-2646.
12. R. O. Al-Kaysi, T. H. Ghaddar and G. Guirado, *Journal of Nanomaterials*, 2009, 2009, 1-14.
13. J. Martín, J. Maiz, J. Sacristan and C. Mijangos, *Polymer*, 2012, 53, 1149-1166.
14. M. S. Fakir, A. Supangat and K. Sulaiman, *Nanoscale research letters*, 2014, 9, 225.
15. A. Supangat, A. Kamarundzaman, N. Asmaliza Bakar, K. Sulaiman and H. Zulfiqar, *Mater. Lett.*, 2014, 118, 103-106.
16. T. H. Wei, M. H. Chi, C. C. Tsai, H. W. Ko and J. T. Chen, *Langmuir : the ACS journal of surfaces and colloids*, 2013, 29, 9972-9978.

17. T.-Y. Chu, S. Alem, S.-W. Tsang, S.-C. Tse, S. Wakim, J. Lu, G. Dennler, D. Waller, R. Gaudiana and Y. Tao, *Appl. Phys. Lett.*, 2011, 98, 253301.
18. C. Sekine, Y. Tsubata, T. Yamada, M. Kitano and S. Doi, *Science and Technology of Advanced Materials*, 2014, 15, 034203.
19. T. N. Ng, W. S. Wong, M. L. Chabinyc, S. Sambandan and R. A. Street, *Appl. Phys. Lett.*, 2008, 92, 213303.
20. Y. Gu, C. Wang and T. P. Russell, *Advanced Energy Materials*, 2012, 2, 683-690.
21. W. C. Tsoi, D. T. James, J. S. Kim, P. G. Nicholson, C. E. Murphy, D. D. Bradley, J. Nelson and J. S. Kim, *J. Am. Chem. Soc.*, 2011, 133, 9834-9843.
22. O. V. Botalina, L. N. Sidorov, A. Y. Borshchevsky and E. V. Skokan, *Rapid Commun. Mass Spectrom.*, 1993, 7, 1009-1011.
23. B. C. Y. a. R. Kumar, *International Journal of Nanotechnology and Applications*, 2008, 2, 15-24.
24. S. A, Gevorgyan and F. C. Krebs, in *Handbook of Thiophene-Based Materials: Applic ations in Organic Electronics and Photonics*, eds. I. g. F. Perepichka and D. m. i. F. P. e. r. e. p. hka, John Wiley & Sons, Ltd., 2009, ch. 18, pp. 673-693.
25. C. W. Lee, T. H. Wei, C. W. Chang and J. T. Chen, *Macromol. Rapid Commun.*, 2012, 33, 1381-1387.
26. R. Liu, J. Duay, T. Lanea and S. B. Lee, *PCCP*, 2010, 12, 4309–4316.
27. C. Kästner, D. A. M. Egbe and H. Hoppe, *J. Mater. Chem. A*, 2015, 3, 395-403.
28. B. J. Schwartz, *Annual review of physical chemistry*, 2003, 54, 141-172.
29. R. Q. Yang, Tian, R.Y., Hou, Q., Yang, W. and Cao, Y., *Macromolecules*, 36, 7553-7460.
30. R.-s. Liu, W.-j. Zeng, B. Du, W. Yang, Q. Hou, W. Shi, Y. Zhang and Y. Cao, *Chinese Journal of Polymer Science* 26, 231-240.
31. T.-Q. Nguyen, V. Doan and B. J. Schwartz, *J. Chem. Phys.*, 1999, 110, 4068-4078.
32. F. Provencher, N. Berube, A. W. Parker, G. M. Greetham, M. Towrie, C. Hellmann, M. Cote, N. Stingelin, C. Silva and S. C. Hayes, *Nature communications*, 2014, 5, 4288.
33. S. Falke, P. Eravuchira, A. Materny and C. Lienau, *Journal of Raman Spectroscopy*, 2011, 42, 1897-1900.